J Mater Sci: Mater Med (2012) 23:1961–1969
DOI 10.1007/s10856-012-4668-5

Radiolabeled gelatin type B analogues can be used for non-invasive visualisation and quantification of protein coatings on 3D porous implants

Ken Kersemans · Tim Desmet · Christian Vanhove · Peter Dubruel · Filip De Vos

Received: 16 January 2012 / Accepted: 27 April 2012 / Published online: 9 May 2012

Abstract This study covers the quantification of the covalent attachment of gelatin type B (GelB) and the subsequent adsorption of Fibronectin (Fn) on poly-ε-caprolactone (PCL) surfaces, functionalised with 2-aminoethyl methacrylate (AEMA) by means of post-plasma UV-irradiation grafting. As typical surface characterisation tools do not allow quantification of deposited amounts of GelB or Fn, radiolabeled analogues were used for direct measurement of the amount of immobilized material. Bolton-Hunter GelB (BHG) and Fn were radioiodinated with ^{131}I and ^{125}I respectively and S-Hynic GelB (SHG) was labeled with ^{99m}Tc. Immobilisation of ^{131}I-BHG or ^{99m}Tc-SHG on both PCL and PCL-AEMA scaffolds was performed in analogy with earlier work. SPECT images on scaffolds coated with ^{99m}Tc-SHG conjugates were acquired on a U-SPECT II camera. There was a clear difference in the amount of deposited ^{131}I-BHG between blanco and AEMA-grafted PCL on 2D samples. No significant differences in immobilization behaviour were observed between ^{99m}Tc-SHG and ^{131}I-BHG. Subsequent immobilisation of Fn was successful and depended on the amounts of deposited GelB. SPECT imaging on cylindrical 3D scaffolds confirmed these findings and showed that the amount of immobilized ^{99m}Tc-SHG was depth dependant. The architecture of the scaffolds strongly influences the distribution of GelB within these structures. Furthermore, there is a clear difference in the homogeneity of the protein coating when different GelB immobilization protocols were applied. This study shows that radiolabeled compounds are a rapid and accurate tool in the quantitative and qualitative evaluation of the biofunctionalisation of AEMA grafted PCL scaffolds.

Ken Kersemans, Tim Desmet contributed equally to this publication.

K. Kersemans (✉) · F. De Vos
Laboratory for Radiopharmacy, Gent University,
Harelbekestraat 72, 9000 Ghent, Belgium
e-mail: ken.kersemans@ugent.be

T. Desmet · P. Dubruel
Polymer Chemistry and Biomaterials Research Group,
Gent University, Ghent, Belgium

C. Vanhove
Department IBITech-MEDISIP-INFINITY-GROUP-ID
Consortium, Gent University, Ghent, Belgium

1 Introduction

Tissue engineering is an emerging scientific field which aims to develop biological substitutes that restore, maintain, or improve tissue function or even reconstruct a whole organ [1]. Scientific advances in the fields of biomaterials and stem cell-research together with the increased knowledge on growth and differentiation factors and biomimetic environments have created unique opportunities to develop tissues in the laboratory from combinations of engineered extracellular matrices ("scaffolds"), cells, and biologically active molecules [2]. An overview of the general strategy to create these tissues is outlined in Fig. 1. Briefly, a biodegradable scaffold is produced that enables temporary support for the development of new tissue either through tissue invasion in the scaffold or through cells cultured on the scaffold prior to implantation. More recently, Computer-Aided Design and Computer-Aided Manufacturing (CAD/CAM) strategies are applied to create patient-specific 3D porous implants by the use of additive manufacturing (AM). The latter has attracted a lot of attention especially when additive manufacturing of poly-ε-caprolactone (PCL) is combined with osteoconductive mineral

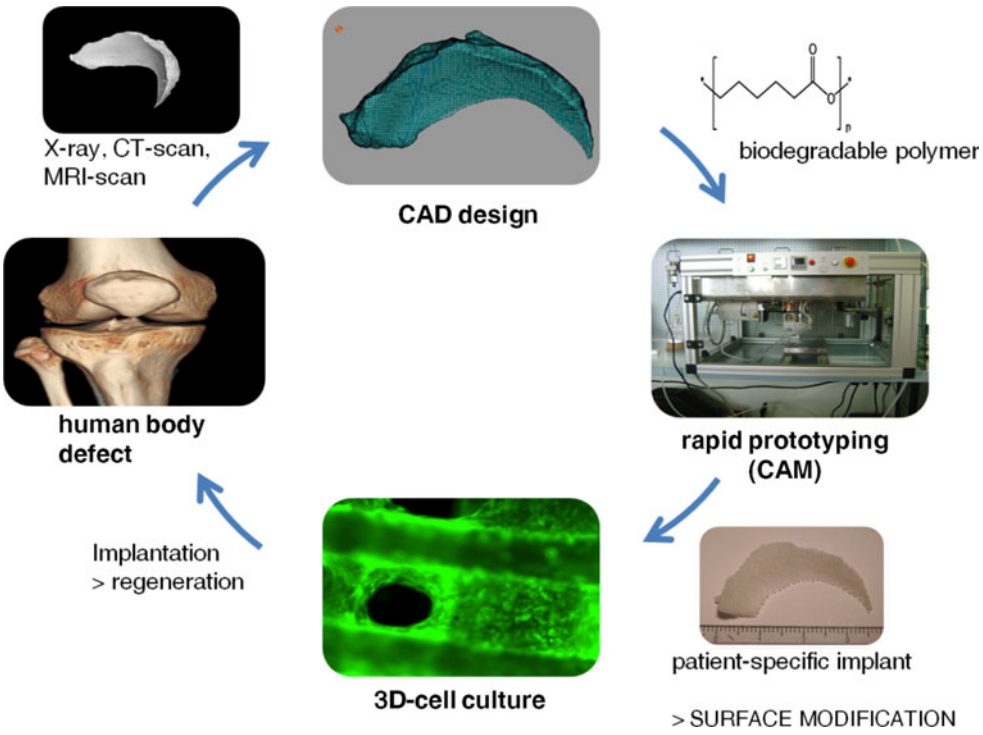

Fig. 1 A schematic representation of the general strategy in scaffold-based tissue-engineering. In a first step imaging of a defect is performed. The 3D-image from CT or MRI data can then be processed into a CAD-design. This design can be used to produce a patient-specific biodegradable implant by additive manufacturing. If necessary, surface modification and cell-culture might be performed prior to implantation

materials such as hydroxyapatite (HA) or tricalciumphosphate.

PCL is a hydrophobic, semi-crystalline, biodegradable or bioresorbable polyester and its crystallinity tends to decrease with increasing molecular weight. The good solubility of PCL in several organic solvents, its low melting point (59–64 °C), low economic cost and exceptional blend-compatibility has stimulated extensive research into its potential application in the biomedical field [3–14]. However, a drawback is its hydrophobic nature, the poor cell attachment and poor proliferation rate [15–18]. Consequently, several surface modification strategies have been investigated in order to enhance cell adhesion and improve the biocompatibility of PCL [15–29]. Most of these surface-modification strategies involve the immobilization of a biomolecule on the surface of the implant [27], which is mostly studied on 2D-polymer films. However, 3D information is still lacking and reports describing the surface modification of 3D scaffolds produced by additive manufacturing are rare. Yildirim et al. [28] revealed that a combined effect of plasma treatment and fibronectin (Fn) adsorption increased the osteogenic differentiation of cells on 3D PCL-scaffolds. Another group reported that a collagen coating on PCL/TCP scaffolds improved both the cell-attachment and cell-viability [29]. Both groups used X-ray photoelectron spectroscopy, scanning electron microscopy and atomic force microscopy to study the coating on the struts [28, 29]. Although these findings are very promising, to the best of our knowledge no methods are available to quantify the chemical immobilisation of gelatin type B (GelB), on 2D-polymer films or on different AM PCL scaffolds nor to assess the homogeneity of the coating.

We report on the quantification of the chemical immobilization of gelatin type B (GelB), on 2D-polymer films as well as on different AM PCL scaffolds and the study of adsorption of Fn on the resulting biofunctionalized surfaces. The rationale behind this set-up is based on the fact that several subunits of Fn possess a binding site for gelatin, a feature that is already being exploited in the chromatographic separation of Fn from plasma and serum [30]. To overcome the shortcomings of aforementioned spectroscopy and microscopy techniques, radiolabeled analogues of GelB and Fn will be used to allow direct measurement of the amounts of immobilized materials by means of activity measurements and Single Photon Emission Tomography (SPECT) data. The latter technique can provide quantitative information on the spatial (3D) distribution of radiolabeled GelB or Fn within the porous implants. A comprehensive review on the state of the art of the molecular SPECT, describing strengths and weaknesses and focusing on different SPECT designs and detection systems was published by Khalil et al. [31]. Finally we will study whether this experimental setup allows the assessment of the degree of homogeneity of the immobilised biopolymer coating.

2 Materials and methods

2.1 Preparation of the 2D samples and 3D scaffolds

An overview of all used samples and scaffolds is given in Table 1. The analytical methods described in this work are first evaluated on small 2D scaffolds, followed by experiments on small and large 3D scaffolds. The latter are used for a proof of principle study, using SPECT imaging.

The detailed method for the development of two-dimensional (2D) samples was published earlier by Desmet et al. [32]. Briefly, the samples were prepared by coating glass cover slips (diameter 25 mm) with a thin PCL film by spincoating. Following treatment with argon plasma the pre-activated strips were grafted with aminoethyl methacrylate (AEMA) to enable covalent linking of GelB. The resulting surfaces are referred to as PCL-AEMA and PCL-GelB, respectively. Finally, Fn is physisorbed onto the GelB layer which resulted in a double protein coating referred to as PCL-Fn.

The method as described by Lee et al. [33] was used for the fabrication of the porous three-dimensional (3D) scaffolds, except that for the functionalization of the PCL surface the same method was used as for the 2D scaffolds. Three types of 3D scaffolds were prepared. First, small cylindrical scaffolds with a height of 3 mm and a diameter of 4.5 mm were used. The strut diameter was determined to be 220 μm, whereas the average pore size was 250 μm. These pores were created with a lay-down pattern of 0/90° creating open channels throughout the structure. This results in a calculated porosity of 63 %. For the visualization experiments larger cylindrical scaffolds with the same lay-down pattern were used. These cylinders feature an overall diameter of 20 mm and a height of 10 mm. The porosity is consequently also 63 %. Finally, a more realistic scaffold was based on the CT-image of a bone structure of a mouse (see figure). These scaffolds have a width of 24 mm and a height of 10 mm. The strut diameter was 220 μm, but the pore size was 480 μm. However, as a shifted pattern was applied, the channels in the z-direction were obstructed for these structures. The porosity of these scaffolds is 75 %.

Table 1 A summary of all used samples, listed with their amounts and role in the study

Type of sample	Amount	Purpose
Small 2D discs	6	Samples for GelB immobilisation study (Blanco)
	6	Samples for GelB immobilisation study (AEMA grafted)
	6	Fn Physisorption on PCL
	6	Fn Physisorption on PCL-GelB
	6	Fn Physisorption on PCL-AEMA-GelB
Small 3D scaffold	4	Immobilisation of 131I-BHG
	4	Immobilisation of 99mTc-SHG
Large 3D scaffold (cylinder)	2	SPECT imaging on Blanco scaffolds coated with 99mTc-SHG (2 protocols)
	2	SPECT imaging on AEMA grafted scaffolds coated with 99mTc-SHG (2 protocols)
Large 3D scaffold (bone mimetic)	2	Proof of principle SPECT imaging on AEMA grafted scaffolds coated with 99mTc-SHG (2 protocols)

2.2 Synthesis of Bolton-Hunter Gelatine B (BHG)

Thirty milligrams of Gelatin type B (Sigma–Aldrich, Belgium) was added to 3 mL Borax buffer (0.1 M, pH 9, 37 °C), containing 1 mg water soluble Bolton-Hunter reagent (Thermo Scientific, USA). The suspension was stirred gently and maintained at 37 °C until all GelB was in solution. From this point onwards, the reaction was allowed to proceed at room temperature for 3 h. Next, the reaction mixture was transferred into a 3 mL slide-a-lyser cassette (Thermo Scientific, USA) and was dialysed in 500 mL of a 0.01 M phosphate buffer of pH 7 at room temperature. At 2 and 4 h post initiation, the buffer was refreshed, after which dialysis was allowed to proceed overnight. The next morning, the solution was transferred into a 20 mL glass vial from which a sample was taken for a Bradford protein essay. Finally, the solution was diluted with PBS (0.01 M, pH 7) to a concentration of 5 mg/mL (BHG stock solution), which was stored at 5 °C prior to use.

2.3 Synthesis of S-Hynic Gelatine B (SHG)

Thirty milligrams of GelB (Sigma–Aldrich, Belgium) was added to 2.95 mL of a 8.4 % sodium hydrogen carbonate (pH 7.5) solution at 37 °C and the suspension was stirred gently until all GelB was in solution. One mg S-Hynic reagent (ABX, Germany) was dissolved in 50 μL DMSO and added to the GelB solution in 10 μL portions of over a time span of 5 min, after which the reaction was allowed to proceed for 30 min in the dark, while maintaining the solution at 37 °C. Before the solution was dispensed in two 3 mL Slide-A-lyzer cassettes (Thermo Scientific, USA), 3 mL of a 0.15 M acetate buffer was added to the reaction mixture. Dialysis was performed at room temperature as described above, using a 0.15 M acetate buffer (pH 7). The final 5 mg/mL SHG stock solution, which was stored at 5 °C prior to use.

2.4 ^{131}I labeling of BHG

Radioiodination was performed as described by Pierce Biotechnology Inc. (Rockford, IL, USA; www.piercenet.com). Iodogen (1,3,4,6-tetrachloro-3a,6a-diphenylglycouril, Pierce, USA) was dissolved in chloroform to a concentration of 2 mg/mL and 100 µL was added to an 1.5 mL conical vial. Chloroform was evaporated under a gentle N_2 flow at room temperature, hereby coating the Iodogen onto the inner surface of the vial. The Iodogen coated vials were stored in a dessicator at 5 °C prior to usage.

To a Iodogen coated reaction vessel was added 0.5 mL of BHG stock solution, immediately followed by 10–20 µL radioiodide solution in 0.05 N NaOH (^{131}I: GE/Amersham Health, Eindhoven, The Netherlands). This mixture was incubated at ambient temperature under slight shaking. The overall radiochemical purity (RCP) was determined using iTLC-SG chromatographic strips (Gelman Sciences) and citrate-buffer (0.068 M citrate, pH 7.4) as eluent. Free iodine was removed by G-25 Sephadex gel filtration (GE Healthcare, Belgium) equilibrated with 0.01 M PBS buffer of pH 7. The concentration of BHG in the final solution was adjusted to 1 mg/mL. The stability of ^{131}I-BHG was checked 8 h later, using the abovementioned iTLC method.

2.5 ^{99m}Tc labeling of SHG

Hynic modified GelB (500 µL of SHG stock solution) was radiolabeled with ^{99m}Tc by the addition of 25 µL tricine stock solution (4 mg/mL in 0.9 % NaCl), 25 µL of Tin(II)sulphate stock solution (0.2 mg/mL in 0.9 % NaCl) and 0.5 mL generator eluate ($[^{99m}TcO_4]^-$, 1.3 GBq). The solution was incubated for 30 min at room temperature. The reaction mixture was analyzed using iTLC-SG chromatographic strips (Gelman Sciences) with either acetone as the mobile phase to determine the percentage of $^{99m}TcO_4^-$ or citrate-buffer (0.068 M citrate, pH 7.4) for the overall RCP. Finally, ^{99m}Tc-SHG was purified by gel filtration through a G-25 Sephadex column (GE Healthcare, Belgium), equilibrated with 0.01 M PBS buffer of pH 7. The concentration of SHG in the final solution was adjusted to 1 mg/mL. The stability of ^{99m}Tc-SHG was determined as above.

2.6 Radiosynthesis of ^{125}I-Fibronectin (^{125}I-Fn)

Fn was labeled with ^{125}I using the Iodogen method that was previously described [34], except that aqueous ^{125}I-Fn solutions were prepared in a concentration of 1 mg/mL.

2.7 Immobilisation of radiolabeled GelB analogues on the PCL-AEMA surfaces

Two coating strategies were compared. First, physisorption of GelB was investigated on untreated PCL surfaces. Secondly, the covalent immobilisation of radiolabeled GelB analogues onto PCL-AEMA films was studied. Both methods were described earlier[32] for non-radioactive GelB immobilisation on 2D surfaces and were applied as such. For the study on the 2D surfaces, all experiments were repeated six times. For the 3D scaffolds two different protocols were used for the immobilisation of ^{99m}Tc-SHG, based on the method for the 2D films. In a first protocol, samples were incubated in solution at rest and under atmospheric pressure (protocol 1) while in the second protocol, the samples were stirred and maintained under vacuum (protocol 2). For the small 3D structures, 4 scaffolds were used for each experiment. For the large 3D structures only one scaffold was used for each experiment.

Quantification of the amount of immobilised radiolabeled GelB analogue was performed by measuring the sample associated activity (2D samples and porous 3D scaffolds) using a dose calibrator (CAPINTEC CRC-15R, Capintec Instruments, USA) or by acquiring SPECT images of the samples (only 3D scaffolds) as described below.

2.8 Immobilisation of radiolabeled ^{125}I-Fn

Samples, previously treated with SHG or BHG, were immersed in 2 mL of a 1 mg/mL ^{125}I-Fn solution for 60 s and dried at the atmosphere in a 6-well plate. The amount of incorporated ^{125}I-Fn was obtained by counting the radioactivity on the samples in a dose calibrator.

2.9 SPECT imaging

SPECT acquisitions were performed to provide 3D images [31] of the distribution of ^{99m}TC-SHG within the scaffolds. The ^{99m}TC-SHG-coated scaffolds were imaged on a MiLabs U-SPECT-II/CT. A 1.0 mm rat collimator was used, featuring 75 pinholes of 1 mm, focusing on a single volume (diameter = 27 mm, 11 mm axial). The spatial resolution that can be obtained with this imaging system is 0.8 mm. By translation of the bed into the three spatial directions a field of view (FOV) of 27 × 22 × 38 mm (x y z) was obtained. The total scan time for each SPECT acquisition was 20 min and the data were recorded in list mode. From the list-mode data, only the photons with an energy of 140 keV ± 20 % were selected. All data were reconstructed with OS-EM using six iterations in combination with 16 subsets. The voxel size in the reconstructed images was 0.75 mm.

The activity (activity range between 7.0 and 52 MBq) on the scaffolds was measured in a dose calibrator. Assessment of the activity distribution on the scaffolds was achieved by drawing volumes of interest (VOI) [35] in the medical imaging data analysis program Amide (VA Linux Systems). An elliptical VOI (diameter = 20 mm, height = 9 mm) was drawn over the whole structure to cover the total activity and smaller ROIs (diameter = 20 mm, height = 1 mm) were drawn to allow the establishment of an activity profile. Normalisation was performed by dividing the measured activity on the scaffold by the total number of counts within the VOI that was drawn over the total structure.

3 Results and discussion

This study ultimately aims to quantify the process of chemical immobilisation of GelB and the subsequent adsorption of Fn on PCL-GelB scaffolds in a 3D set-up. Since typical surface characterisation techniques such as QCM and SPR measurements are limited to monitoring interactions at surfaces in 2D, we propose radiolabeled GelB and Fn as a strategy to allow this quantification. In this study we started with the evaluation of the method on 2D samples and with the acquired knowledge we moved on to porous 3D samples of different sizes and shapes. All data were compared to that of negative controls as the study of the physisorption of GelB to untreated PCL surfaces was part of each experiment.

3.1 Radiolabeling experiments

The radiochemical yields of ^{131}I-BHG, ^{99m}Tc-SHG and ^{125}I-Fn were 73, 93 and 88 % respectively. All labeled compounds were obtained with a RCP >99 % after purification and were stable for at least up to 8 h after production.

3.2 Immobilisation of GelB on 2D samples

First the effect of the post-plasma AEMA grafting on the amount of immobilised GelB was studied on 2D PCL polymer films using ^{131}I-BHG. Untreated PCL films were used as a reference. As Table 2 shows, there is a significant difference between the untreated PCL samples and the PCL-AEMA samples ($n = 6$; $p = 0.019$). This observation shows that the covalent attachment of GelB to the AEMA grafted PCL layer increases the amount of immobilised GelB with 38 % relative to untreated PCL films. Overnight incubation in ultrapure water at 37 °C showed that there is a slight loss of activity due to the release of unbound GelB: either not covalently linked or caught in the matrix of the protein coating. After overnight incubation, the % Relative standard deviation (%RSD) was lower for the AEMA grafted PCL samples (12 %) than for the untreated PCL samples (23 %), indicating that a more reproducible surface is generated when the surface is functionalised with AEMA. Finally, it was shown that the additional clean-up procedure after the initial washing step (overnight incubation of the samples in ultrapure water at 37 °C) did not result in a statistically relevant change of the amounts of immobilised GelB for these 2D-films. Therefore, for the 2D-samples it is sufficient to rinse the samples thoroughly with milliQ.

Table 2 The amounts of immobilised ^{131}I-BHG, both on the untreated PCL and on the PCL-AEMA 2D-films

Incubation at 37 °C	Immobilised GelB (ng/mm^2)	
	Untreated	AEMA
0 h	39.1 ± 4.8	64 ± 14
Overnight	35.0 ± 3.3	57.0 ± 1.5

Data are expressed as average ± std dev ($n = 6$)

3.3 Immobilisation of ^{125}I-Fn on 2D samples

The immobilisation of ^{125}I-Fn was studied on "naked" untreated PCL films (referred to as PCL), as well as on untreated and AEMA grafted PCL films that were coated with GelB (referred to as PCL-GelB and PCL-AEMA-GelB respectively). The "naked" untreated samples showed a relatively low uptake of ^{125}I-Fn (see Table 3), attributed to a non specific adsorption of Fn on the PCL surface. The samples that were already coated with GelB showed an elevated adsorption of ^{125}I-Fn, more than a factor 4 higher (significant difference: $p = 0.003$ and $p = 0.0002$ for PCL-GelB and PCL-AEMA-GelB, respectively) than the samples that were not previously coated with GelB.

Despite the observation that, on average, AEMA grafted samples coated with GelB showed a higher uptake of ^{125}I-Fn than the untreated PCL samples that were coated with GelB, no significant difference could be demonstrated. The ratio of absorbed Fn(ng/mm^2)/immobilised GelB (ng/mm^2) was on average 0.15 ± 0.07.

Table 3 The amounts of immobilised ^{125}I-Fn by physisorption, on the blank PCL and on both types of PCL films with GelB

	Immobilised Fn (ng/mm^2)
PCL	1.47 ± 0.34
PCL-GelB	6.05 ± 2.09
PCL-AEMA-GelB	6.85 ± 1.47

The type PCL-GelB was the blank PCL film with EDC-immobilised GelB, the type PCL-GelB was the PCL-AEMA coated sample with EDC-immobilised GelB. Data are expressed as average ± std dev ($n = 6$)

As for the immobilisation of GelB, the reproducibility of the physisorption of ^{125}I-Fn on the samples was better for the PCL-AEMA films than for the untreated PCL films, reflecting the reproducability of the GelB layers.

On the basis of aforementioned observations, it can be stated that grafting of AEMA increases the amount of GelB that can be immobilised and leads to more reproducible surfaces, both for the GelB immobilisation and the adsorption of Fn. However, it might be so that for initial cell-adhesion purposes a cross-linked layer of GelB on PCL is sufficiently thick and stable. This is suggested in the literature for collagen. Furthermore, the affinity of Fn for GelB is much higher compared to blank PCL (fourfold).

3.4 Immobilisation of GelB on small 3D samples

Next we assessed whether the results obtained on 2D samples are transferrable to 3D-scaffolds. For these tests cylindrical scaffolds were used, measuring 3 mm high and 4.5 mm in diameter with a 0/90° lay-down pattern that is exemplified in Fig. 2. The immobilisation of ^{131}I-BHG as well as ^{99m}Tc-SHG on these 3D PCL-AEMA structures was studied.

First, it is important to note that for these small scaffolds the overnight rinsing is critical as about 25–50 % of the radiolabeled GelB is removed by overnight incubation. As opposed to the 2D-films, GelB is adsorbed or trapped within the pores of the structure and cannot be easily removed by thoroughly rinsing the samples. Overnight incubation allows the unbound GelB to redissolve and to be washed out of the porous structure.

As Table 4 shows, no significant difference ($p = 0.19$) between the amounts of immobilised ^{99m}Tc-GelB and ^{131}I-GelB could be noted after the incubation step. Hence, both constructs show identical coating properties within this experimental set-up.

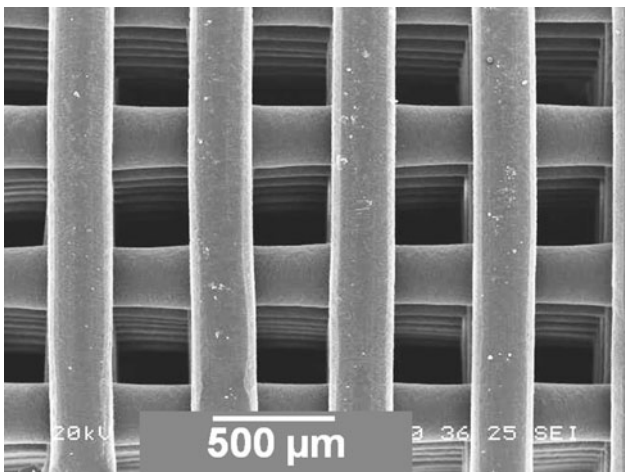

Fig. 2 A scanning electron microscope, *top-view* of cell-substrate scaffolds with 0/90° lay-down pattern which were used for the experiments on 3D scaffolds

Table 4 The amount of immobilised radiolabeledGelB on small cell substrate scaffolds, grafted with AEMA, expressed as the total amount of labelled GelB per scaffold in µg/scaffold ($n = 4$) or normalised in function of available 3D surface in ng/mm^2

	131I BHG	99mTc-SHG
Total (µg/scaffold)	6.3 ± 1.9	4.6 ± 1.3
Normalised (ng/mm^2)	30.0 ± 9.0	21.9 ± 6.2

In comparison with the 2D samples, the small 3D samples show a decrease ($p = 0.006$) in GelB immobilisation per mm^2 with a factor 1.8, due to the more difficult penetration of the solution into the 3D structure, reducing the efficiency of the GelB immobilisation. Despite this trend, sufficient amounts of GelB (the limit of quantification was 0.5 ng GelB/mm^2) are immobilised to allow quantitation and these findings advocate the study of the immobilisation of GelB by its radiolabeled analogue, ^{99m}Tc-GelB, for the quantification and study of the homogeneous character of the GelB coatings by means of radioactivity measurements and SPECT imaging.

3.5 Immobilisation of GelB on large 3D samples

The profile of the immobilized ^{99m}Tc-SHG on PCL and AEMA grafted PCL samples is shown in Fig. 3 and the average amounts of immobilised GelB are presented in Table 5. Depending on the applied immobilisation protocol (with or without stirring and vacuum), some important differences can be observed. The in-depth profile of blanco samples showed that the deposition of ^{99m}Tc-SHG averages 0.0304 ± 0.0065 and 0.03773 ± 0.0050 µg/mm^3 for protocol 1 and protocol 2, respectively ($p = 0.02$), a small but significant difference. Also, the percent relative standard deviation (%RSD) is 21 % for protocol 1 and 13 % for protocol 2. These observations suggest that stirring and degassing is a means achieve a better deposition of GelB within the 3D scaffolds, due to the prevention of air bubbles inside the structures and by improvement of the penetration of the gelatin solution within the structure.

The AEMA grafted samples showed an average ^{99m}Tc-SHG immobilisation of 0.215 ± 0.073 and 0.192 ± 0.075 µg/mm^3 for protocol 1 and protocol 2 respectively. In comparison with the blanco samples, this represents a significant ($p = 6 \times 10^{-5}$) increase of about a factor 7 for both protocols, due to the AEMA grafting. When the deposited amounts of GelB are normalised to the available surface, an increase with a factor 2.7 and 2.4 can be observed for protocol 1 and protocol 2 respectively. This may be due to a more difficult wash out from larger scaffolds.

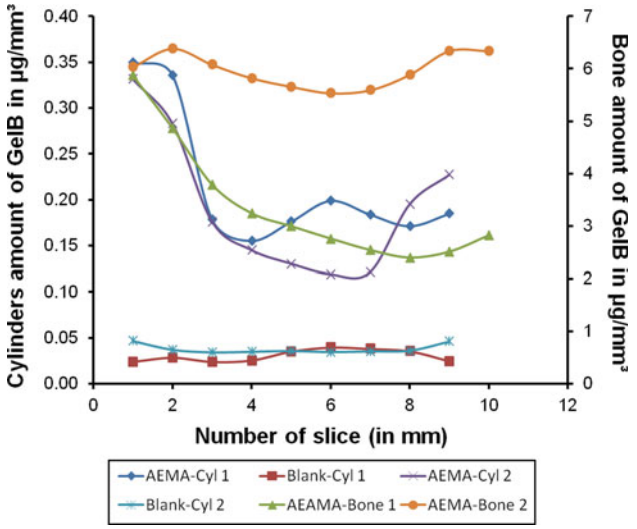

Fig. 3 The depth-profile of the amount of GelB along the *Z*-axis for the different structures Blank-Cyl, AEMA-Cyl and AEMA-Bone, as well as for protocol 1 and for protocol 2. The primary *Y*-axis (*left*) shows the values for the cylindrical scaffolds while the secondary *Y*-axis (*right*) displays the values for the scaffolds that imitate bone structures (featuring a shifted lay down pattern)

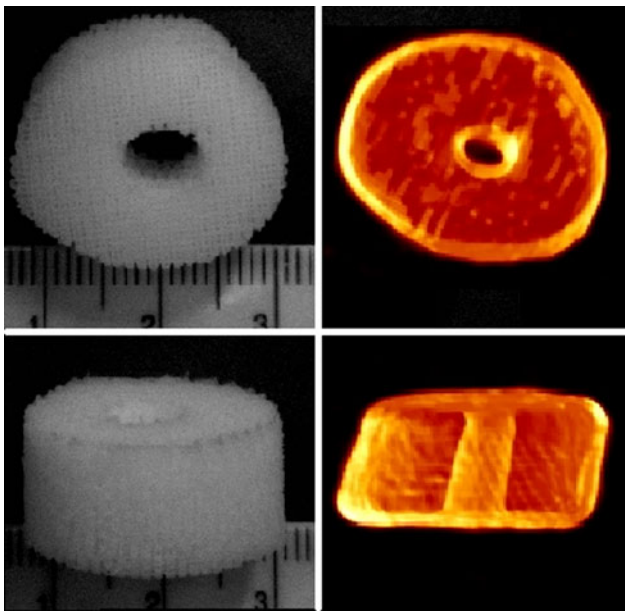

Fig. 4 *Left*: illustration of a 3D scaffold that closely resembles a structure that is to be implanted in in vivo settings. *Right*: a 3D rendering of a representative SPECT acquisition of this scaffold after immobilisation of ^{99m}Tc-SHG

The distribution of ^{99m}Tc-SHG within the 3D scaffold when protocol 2 is applied showed no significant difference ($p = 0.5$) with protocol 1. The %RSD for both protocols is also very similar (34 and 39 % for protocol 1 and 2 respectively). This may be due to the fact that the AEMA grafted surfaces are much less hydrophobic and aqueous solutions easily penetrate the 3D structures. Interestingly, the distribution within the AEMA samples is not symmetrical and shows more ^{99m}TcSHG on one side than on the other. Also, the amounts of deposited ^{99m}TcSHG decrease towards the centre of the structure. As such observation could not be made for the blanco samples and as both protocols yield similar results, this phenomenon is not related to the penetration mechanics of ^{99m}TcSHG within the structure but most likely to an assymetricity specific to the AEMA grafted sample surfaces. As there is a clear link between the presence of AEMA on the surface and the amount of GelB that is immobilised, it is likely that the GelB gradient is linked to a grafting gradient within the 3D structure. This is understandable as the UV light cannot efficiently penetrate the structure. The fact that one side shows a more elevated ^{99m}TcSHG immobilisation than the other can be linked to an assymmetrical irradiation set-up, inherent to the available apparatus.

In a final part of the present work, 3D scaffolds were studied that closely resemble structures that are to be implanted in in vivo settings. The main difference is that the different PCL layers are stacked in such a way that there are no clear pores or channels present as opposed to the structures described in higher paragraphs. These samples showed an average ^{99m}Tc-SHG immobilisation of 3.38 ± 0.79 and 5.97 ± 0.34 µg/mm^3 for protocol 1 and protocol 2 respectively. An example of aforementioned

Table 5 The amount of immobilised GelB on larger scaffolds, in ng/mm^3 and normalized (to the available 3D surface) in µg/mm^2

	Blank-Cyl ($n = 9$ slices)	AEMA-Cyl ($n = 9$ slices)	AEMA-Bone ($n = 10$ slices)
Immobilised GelB (µg/mm^3)			
Protocol 1	0.0304 ± 0.0065	0.215 ± 0.073	3.38 ± 0.79
Protocol 2	0.03773 ± 0.0050	0.192 ± 0.075	5.97 ± 0.34
Normalized Immobilized Gel B (ng/mm^2)			
Protocol 1	8.52 ± 1.82	60 ± 20	892 ± 221
Protocol 2	10.57 ± 1.40	53 ± 21	$1{,}578 \pm 89$
Significantly different?	Yes ($p = 0.02$)	No ($p = 0.5$)	Yes ($p = 2.10^{-4}$)

The statistical comparison between protocol 1 and 2 is shown for each construct

scaffold, together with a representative 3D rendering of a SPECT acquisition thereof is shown in Fig. 4. Relative to AEMA grafted structures, this represents a 16 and 31 fold increase of immobilised ^{99m}Tc-SHG for protocol 1 and 2 respectively. Likely, this increased immobilisation is due to hindrance of fluid flow after immobilisation of the GelB, rendering the wash out of non-covalently bound GelB more difficult. Also, application of protocol 2 leads to an almost two fold increase ($p = 2 \times 10^{-4}$) of immobilised ^{99m}Tc-SHG relative to protocol 1. The influence of the applied immobilisation protocol is easily understood on the basis of our previous experiment, although this time, the effect is more prevalent. From the observed %RSD for both protocols (23 and 6 % for protocol 1 and 2 respectively), stirring under vacuum becomes even more important for obtaining a homogenous distribution of GelB.

4 Conclusions

This study shows that radiolabeled GelB is a rapid and accurate tool in the evaluation of the biofunctionalisation of AEMA grafted PCL scaffolds.

A grafting protocol could be optimised on 2D-films and successfully transferred to 3D-substrates from the same material. Importantly, minor adaptations of the protocol are necessary (vacuum application under stirring) in order to ensure a homogeneous coating of the scaffold. The subsequent adsorption of Fn was proven to be successful.

The presence of AEMA led to higher amounts of immobilised GelB and more reproducible protein layers, both in 2D and 3D. This can be understood by considering the electrostatic attraction between the positively charged free amine groups of the AEMA and the negatively charged GelB.

Furthermore, it was shown that the architecture of the scaffold has a marked influence the amount of immobilised protein.

Radiolabelled GelB does not only allow the quantification of the protein, but enables researchers to assess the homogeneous character of the coating by SPECT. Furthermore, it is expected that other proteins (and even cells) that can be labelled with SPECT isotopes can be studied in a similar way. It is our belief that the applied techniques open up unprecedented possibilities for studying protein functionalisation of porous scaffolds for tissue engineering.

References

1. Langer R, Vacanti JP. Tissue engineering. Science. 1993;260(5110):920–6.
2. Woodruff MA, Hutmacher DW. The return of a forgotten polymer—polycaprolactone in the 21st century. Prog Polym Sci. 2010;35(10):1217–56.
3. Hutmacher DW, Schantz JT, Lam CXF, Tan KC, Lim TC. State of the art and future directions of scaffold-based bone engineering from a biomaterials perspective. J Tissue Eng Regen Med. 2007;1(4):245–60.
4. Chen FL, Zhou YF, Barnabas ST, Woodruff MA, Hutmacher DW. Engineering tubular bone constructs. J Biomech. 2007;40:S73–9.
5. Chim H, Hutmacher DW, Chou AM, Oliveira AL, Reis RL, Lim TC, Schantz JT. A comparative analysis of scaffold material modifications for load-bearing applications in bone tissue engineering. Int J Oral Maxillofac Surg. 2006;35(10):928–34.
6. Endres M, Hutmacher DW, Salgado AJ, Kaps C, Ringe J, Reis RL, Sittinger M, Brandwood A, Schantz JT. Osteogenic induction of human bone marrow-derived mesenchymal progenitor cells in novel synthetic polymer-hydrogel matrices. Tissue Eng. 2003;9(4):689–702.
7. Hoque ME, San WY, Wei F, Li SM, Huang MH, Vert M, Hutmacher DW. Processing of polycaprolactone and polycaprolactone-based copolymers into 3D scaffolds, and their cellular responses. Tissue Eng Part A. 2009;15(10):3013–24.
8. Shor L, Guceri S, Wen XJ, Gandhi M, Sun W. Fabrication of three-dimensional polycaprolactone/hydroxyapatite tissue scaffolds and osteoblast-scaffold interactions in vitro. Biomaterials. 2007;28(35):5291–7.
9. Park SA, Lee SH, Kim WD. Fabrication of porous polycaprolactone/hydroxyapatite (PCL/HA) blend scaffolds using a 3D plotting system for bone tissue engineering. Bioprocess Biosyst Eng. 2011;34(4):505–13.
10. Kokubo T, Kim HM, Kawashita M. Novel bioactive materials with different mechanical properties. Biomaterials. 2003;24(13):2161–75.
11. Ciapetti G, Ambrosio L, Savarino L, Granchi D, Cenni E, Baldini N, Pagani S, Guizzardi S, Causa F, Giunti A. Osteoblast growth and function in porous poly epsilon-caprolactone matrices for bone repair: a preliminary study. Biomaterials. 2003;24(21):3815–24.
12. Chen BQ, Sun K. Mechanical and dynamic viscoelastic properties of hydroxyapatite reinforced poly(epsilon-caprolactone). Polym Test. 2005;24(8):978–82.
13. Leung LH, Di Rosa A, Naguib HE (2010) Physical and mechanical properties of poly(E-Caprolactone)—hydroxyapatite composites for bone tissue engineering applications. Imece2009: Proceedings of the Asme International Mechanical Engineering Congress and Exposition, vol 2, pp 17–23.
14. Nair LS, Laurencin CT. Biodegradable polymers as biomaterials. Prog Polym Sci. 2007;32(8–9):762–98.
15. Cheng ZY, Teoh SH. Surface modification of ultra thin poly (epsilon-caprolactone) films using acrylic acid and collagen. Biomaterials. 2009;25(11):1991–2001.
16. Amato I, Ciapettia G, Pagani S, Marletta G, Satriano C, Baldini N, Granchi D. Expression of cell adhesion receptors in human osteoblasts cultured on biofunctionalized poly-(epsilon-caprolactone) surfaces. Biomaterials. 2007;28(25):3668–78.
17. Duan Y, Wang Z, Yan W, Wang S, Zhang S, Jia J. Preparation of collagen-coated electrospun nanofibers by remote plasma treatment and their biological properties. J Biomater Sci Polym Ed. 2007;18(9):1153–64.
18. Gabriel M, Amerongen GPV, Van Hinsbergh VWM, Amerongen AVV, Zentner A. Direct grafting of RGD-motif-containing peptide on the surface of polycaprolactone films. J Biomater Sci Polym Ed. 2006;17(5):567–77.
19. Ma ZW, He W, Yong T, Ramakrishna S. Grafting of gelatin on electrospun poly(caprolactone) nanofibers to improve endothelial cell spreading and proliferation and to control cell orientation. Tissue Eng. 2005;11(7–8):1149–58.
20. Marletta G, Ciapetti G, Satriano C, Pagani S, Baldini N. The effect of irradiation modification and RGD sequence adsorption on the response of human osteoblasts to polycaprolactone. Biomaterials. 2005;26(23):4793–804.

21. Marletta G, Ciapetti G, Satriano C, Perut F, Salerno M, Baldini N. Improved osteogenic differentiation of human marrow stromal cells cultured on ion-induced chemically structured poly-epsilon-caprolactone. Biomaterials. 2007;28(6):1132–40.
22. Santiago LY, Nowak RW, Rubin JP, Marra KG. Peptide-surface modification of poly(caprolactone) with laminin-derived sequences for adipose-derived stem cell applications. Biomaterials. 2006;27(15):2962–9.
23. Tiaw KS, Goh SW, Hong M, Wang Z, Lan B, Teoh SH. Laser surface modification of poly(epsilon-caprolactone) (PCL) membrane for tissue engineering applications. Biomaterials. 2005;26(7):763–9.
24. Wirsen A, Sun H, Emilsson L, Albertsson AC. Solvent free vapor phase photografting of maleic anhydride onto poly(ethylene terephthalate) and surface coupling of fluorinated probes, PEG, and an RGD-peptide. Biomacromolecules. 2005;6(4):2281–9.
25. Zhu YB, Gao CY, Liu XY, Shen JC. Surface modification of polycaprolactone membrane via aminolysis and biomacromolecule immobilization for promoting cytocompatibility of human endothelial cells. Biomacromolecules. 2002;3(6):1312–9.
26. Zhu YB, Gao CY, Shen JC. Surface modification of polycaprolactone with poly(methacrylic acid) and gelatin covalent immobilization for promoting its cytocompatibility. Biomaterials. 2002;23(24):4889–95.
27. Desmet T, Morent R, Geyter ND, Leys C, Schacht E, Dubruel P. Nonthermal plasma technology as a versatile strategy for polymeric biomaterials surface modification: a review. Biomacromolecules. 2009;10(9):2351–78.
28. Yildirim ED, Besunder R, Pappas D, Allen F, Guceri S, Sun W. Accelerated differentiation of osteoblast cells on polycaprolactone scaffolds driven by a combined effect of protein coating and plasma modification. Biofabrication. 2010;2(1):014109.
29. Lee H, Kim G. Three-dimensional plotted PCL/beta-TCP scaffolds coated with a collagen layer: preparation, physical properties and in vitro evaluation for bone tissue regeneration. J Mater Chem. 2011;21(17):6305–12.
30. Ruckenstein E, Guo W. Cellulose and glass fiber affinity membranes for the chromatographic separation of biomolecules. Biotechnol Prog. 2004;20(1):13–25.
31. Khalil MM, Tremoleda JL, Bayomy TB, Gsell W (2011). Molecular SPECT imaging: an overview. Int J Mol Imag. Article ID 796025, 15 pages.
32. Desmet T, Billiet T, Berneel E, Cornelissen R, Schaubroeck D, Schacht E, Dubruel P. Post-plasma grafting of AEMA as a versatile tool to biofunctionalise polyesters for tissue engineering. Macromol Biosci. 2010;10:1484–94.
33. Lee H, Kim GH. Three-dimensional plotted PCL/β-TCP scaffolds coated with a collagen layer: preparation, physical properties and in vitro evaluation for bone tissue regeneration. J Mater Chem. 2011;21:6305–12.
34. Van Vlierberghe S, Vanderleyden E, Dubruel P, De Vos F, Schacht E. Affinity study of novel gelatin cell carriers for fibronectin. Macromol Biosci. 2009;9(11):1105–15.
35. Zaidi H, Hasegawa BH. Quantitative analysis in nuclear medicine imaging. New York: Springer; 2006.